Influence of the substrate on the spin-orbit splitting in surface alloys on (111) noble-metal surfaces

L. Moreschini,[1] A. Bendounan,[2,3] H. Bentmann,[2] M. Assig,[4] K. Kern,[1,4] F. Reinert,[2,5] J. Henk,[6] C. R. Ast,[4] and M. Grioni[1]
[1]*Ecole Polytechnique Fédérale de Lausanne (EPFL), Institut de Physique de la Matière Condensée, CH-1015 Lausanne, Switzerland*
[2]*Experimentelle Physik II, Universität Würzburg Am Hubland, D-97074 Würzburg, Germany*
[3]*Synchrotron Soleil, L'Orme des Merisiers, Saint-Aubin, BP 48, F-91192 Gif-sur-Yvette Cedex, France*
[4]*Max-Planck-Institut für Festkörperforschung, D-70569 Stuttgart, Germany*
[5]*Forschungszentrum Karlsruhe, Gemeinschaftslabor für Nanoanalytik, D-76021 Karlsruhe, Germany*
[6]*Max-Planck-Institut für Mikrostrukturphysik, Weinberg 2, D-06120 Halle (Saale), Germany*
(Received 2 March 2009; revised manuscript received 2 July 2009; published 31 July 2009)

We have studied by angle-resolved photoelectron spectroscopy the ordered $X\mathrm{Cu}_2$ surface alloys formed by X=Sb and Bi on a Cu(111) substrate. We found clear analogies with the corresponding $X\mathrm{Ag}_2$ alloys formed by the same elements on Ag(111). The electronic states near the Fermi level are similarly split by the spin-orbit (SO) interaction with the smaller splitting in $X\mathrm{Cu}_2$ reflecting the smaller atomic SO parameter of Cu vs Ag. The charge transfer from the Bi and Sb adatoms to the substrate atoms and their outward relaxation are different for two substrates; both determine the Fermi energy of the two-dimensional electron gas.

DOI: 10.1103/PhysRevB.80.035438 PACS number(s): 73.20.At, 79.60.−i, 71.70.Ej

I. INTRODUCTION

In three-dimensional solids the degeneracy of opposite spin states is removed by the spin-orbit (SO) interaction for space groups lacking an inversion center. At surfaces, on the other hand, the lifting of the spin degeneracy is intrinsically allowed by the structural inversion asymmetry along the surface normal. The possibility of an in-plane asymmetry is usually not considered but recent results on binary surface alloys have reported energy and wave-vector separations much larger than found in either of the constituents.[1,2] This has been substantiated by a model approach[3] and by first-principles calculations.[2,4] The coexistence of a normal and an in-plane component of the surface-potential gradient yields an unmatched splitting, which is supported by the strong confinement of the electronic wave functions at the interface.

Surface alloys formed by p metals (Sb, Pb, and Bi) on Ag(111) have been recently studied by angle-resolved photoelectron spectroscopy (ARPES). The splitting increases with the atomic number Z of the constituents from Sb (Ref. 5) to Bi.[2] This confirms the major role played by the atomic SO parameter in determining the strength of the splitting, predicted by theoretical arguments,[6,7] and illustrated by experimental work on clean noble-metal surfaces.[8–10] Concerning the substrate, among noble metals the largest effect would be expected for Au, whose large SO interaction is evidenced by the splitting of its Shockley surface state but the herringbone surface reconstruction of Au(111) seems to prevent alloy formation.

In order to assess the influence of the substrate on the surface electronic structure, we set out to study the Sb/Cu(111) and Bi/Cu(111) surface alloys. At 1/3 monolayer (ML) coverage both Bi and Sb form on Cu(111)—like on Ag(111) (Refs. 5 and 11)—one-layer-thick alloys with a $(\sqrt{3}\times\sqrt{3})R30°$ structure. The stoichiometry is $X\mathrm{Cu}_2$ (X=Sb and Bi).[12–15] Hence, the electronic structures of the BiCu_2 and SbCu_2 systems lend themselves to a direct comparison with those of their sister compounds on Ag(111). In contrast, Pb on Cu(111) does not form a long-range-ordered alloy with 1/3 ML coverage[16] and is therefore not considered here.

The results for surface alloys published so far are interpreted in terms of the Rashba-Bychkov model.[17] The band structure of an ideal two-dimensional electron gas (2DEG) around the $\bar{\Gamma}$ point ($\vec{k}_{\parallel}=0$) of the surface Brillouin zone (BZ) within this framework is shown in Fig. 1. A cut along a line through $\bar{\Gamma}$ gives a characteristic dispersion of two split parabolas,

$$E_{\pm}(\vec{k}) = E_0 + \frac{\hbar^2 k^2}{2m^\star} \pm \alpha_R |k|, \tag{1}$$

in which we define $k_0=\alpha_R m^\star/\hbar^2$ as the momentum offset of the band maximum. The Rashba energy E_R is given by the

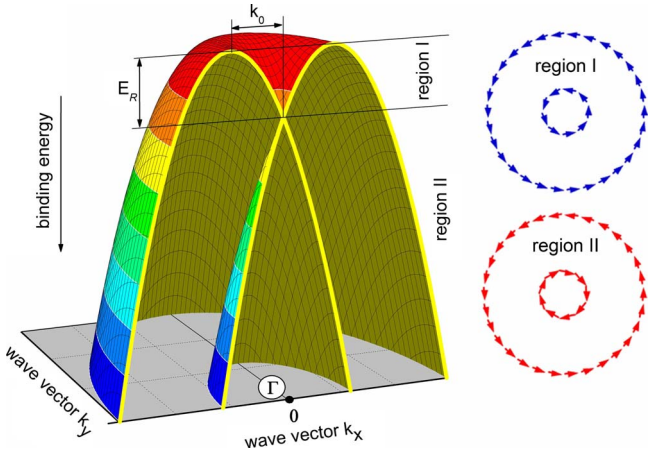

FIG. 1. (Color online) Schematic of the band dispersion resulting from the lifting of the spin degeneracy at the surface. The crossing point at $\bar{\Gamma}$ defines two different regions: region I, where the constant energy contours have the same helicity and the DOS follows a $1/\sqrt{E}$ behavior and region II, where the contours have opposite helicities and the DOS is constant as in a conventional 2DEG.

energy difference between $E(k_0)$ and the crossing point at $\bar{\Gamma}$, E_0. The Rashba parameter α_R, which is proportional to the potential gradient, is the SO-coupling constant in the Hamiltonian and can be expressed as $\alpha_R = 2E_R/k_0$. Although this simple scenario does not capture important details of the ARPES data,[2–4] it allows an immediate comparison of the splitting in different materials. The parameter α_R should be considered as a measure of the effective electric field in the surface layer, accounting for both the in-plane and the perpendicular potential gradients.

The band dispersion sketched in Fig. 1 can be divided in two qualitatively different regions, depending on the position of the Fermi level E_F with respect to the crossing point E_0. If E_F lies below E_0, in region II, the Fermi energy is larger than the Rashba energy ($E_F > E_R$), with energies being measured from the band maximum. A constant energy cut identifies two surfaces of opposed spin helicity and the density of states (DOS) does not differ from that of the case without SO coupling. If E_F lies in region I the Fermi level is between the band maximum and E_0, leading to $E_R > E_F$. Here, the two surfaces have identical helicity and the DOS switches to a $1/\sqrt{E}$ behavior.[18,19] Moreover, the ratio E_R/E_F cannot be regarded as a "small parameter" in the usual perturbative description of the interacting electron liquid, since $E_R/E_F > 1$, with anomalous consequences on quasiparticle properties.[18,20]

In Bi/Ag(111) the band is fully occupied and therefore E_F is not defined while in Pb/Ag(111) the Fermi level is located in region II. A gradual shift into region I has been achieved in a mixed $Bi_xPb_{1-x}/Ag(111)$ alloy[21] but the surface preparation is complex and introduces chemical disorder. Due to the substrate-dependent relaxation and charge transfer at the interface, replacing Ag(111) by Cu(111) may offer an interesting opportunity of shifting the Fermi level across the band.

II. EXPERIMENTAL DETAILS

A clean ordered Cu(111) surface was prepared by repeated cycles of Ar^+ sputtering and annealing at 800 K.

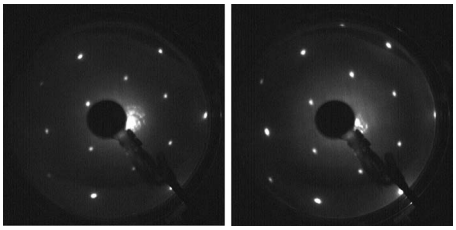

FIG. 2. $(\sqrt{3}\times\sqrt{3})R30°$ LEED pattern of (a) Bi/Cu(111) and (b) Sb/Cu(111). The horizontal axis is along the $\bar{\Gamma}\bar{K}$ direction of the alloys.

Evaporation on the hot substrate ($T > 400$ K) of 1/3 monolayer of Sb or Bi from a Knudsen cell yields an ordered $(\sqrt{3}\times\sqrt{3})R30°$ structure. Both Bi and Sb occupy substitutional sites on Cu(111) at 1/3 monolayer coverage. The stacking of the mixed surface layer is preferentially hcp for Sb (Refs. 13 and 22) and fcc for Bi.[12] In both cases the surface BZ is hexagonal with $\bar{\Gamma}\bar{K} = 0.95$ Å^{-1} and $\bar{\Gamma}\bar{M} = 0.82$ Å^{-1}. The quality of the surface was verified by low-energy electron diffraction (LEED; Fig. 2).

ARPES measurements were performed with a high-brightness monochromatized helium lamp and a high-resolution hemispherical analyzer (Gammadata R4000). The energy resolution was 3 meV and the angular resolution 0.3°. For low-temperature measurements, the surface was repeatedly "refreshed" by a mild annealing ($T \simeq 400$ K).

III. RESULTS AND DISCUSSION

ARPES intensity maps of the $SbCu_2$ and $BiCu_2$ alloys, measured in the $\bar{\Gamma}\bar{M}\bar{\Gamma}$ direction over a wide wave-vector range, are shown in Fig. 3. They are compared to the corresponding ARPES maps of $SbAg_2$ and $BiAg_2$ alloys ($\bar{\Gamma}\bar{K} = 0.84$ Å^{-1} and $\bar{\Gamma}\bar{M} = 0.72$ Å^{-1}). In the Sb alloys (left panels) two bands (A and B) with negative effective masses can be identified, centered at $\bar{\Gamma}$. Each band is expected to be SO

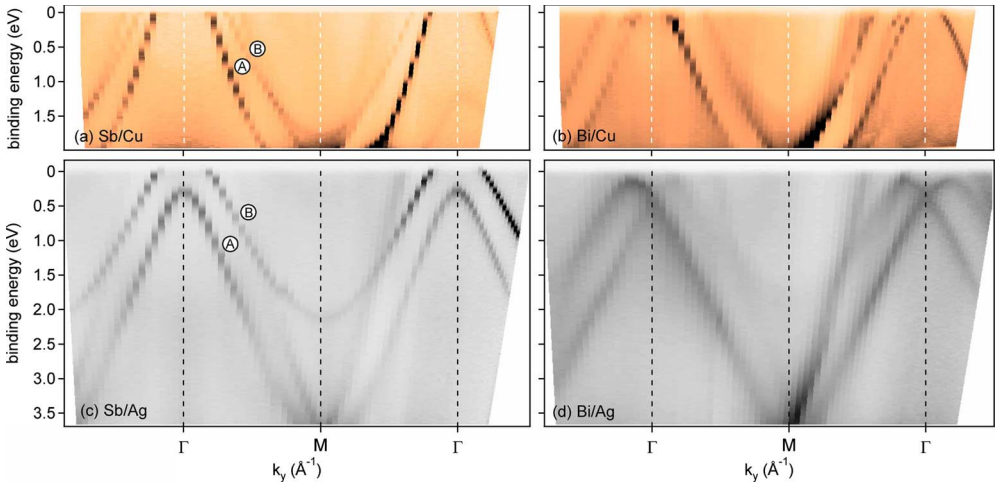

FIG. 3. (Color online) Experimental band dispersion of (a) Sb/Cu(111), (b) Bi/Cu(111), (c) Sb/Ag(111), and (d) Bi/Ag(111), measured at room temperature. The wave-vector axes are rescaled in order to align horizontally the high-symmetry points $\bar{\Gamma}$ and $\bar{M}$ of the Cu and Ag alloys. Note the different energy ranges in the top and the bottom panels. For higher binding energies the intense Cu *d* bands overwhelm all other features.

TABLE I. Relaxation, charge transfer for the Sb(Z=51) and Bi(Z=83) adatoms in the surface alloys, and binding energy $E(sp_z)$ of the sp_z band maximum relative to the Fermi-level position, obtained from our first-principles calculations. The relaxation is given in units of the interlayer distance in the substrate's bulk and Δn is the charge transfer from the adatom (Bi and Sb) to the surrounding, in units of the electron charge.

Alloy	Relaxation (%)	Δn	$E(sp_z)$ (eV)
Sb/Ag(111)	10	0.47	0.30
Bi/Ag(111)	15	0.82	0.31
Bi/Cu(111)	38	1.93	−0.17

split. The splitting is extremely small for both substrates but it has been experimentally resolved for Sb/Ag(111).[5] By analogy with the case of $BiAg_2$, A and B are known to have mainly sp_z and p_xp_y character, respectively.[4] The Bi alloys (right panels) indeed present a similar band structure but with a sizable splitting. The sp_z states consist of two replicas, which are actually more visible in the second BZ. The p_xp_y bands cannot be clearly identified in these large-scale maps. The band dispersion shows a minimum in correspondence of the $\bar{M}$ point, which is a saddle point, as already shown explicitly for the case of Pb/Ag(111).[1] The data on the Sb alloys, where bands A and B have more similar intensities with respect to their Bi counterparts, allow the saddle point to be assigned to the p_xp_y states, rather than to the sp_z band, as suggested elsewhere.[4,23] Free-electronlike bands associated with Cu (Ag) bulk $4s(5s)$ states, dispersing in the second BZ, together with fainter replicas in the first BZ, are observed in all four ARPES maps. An analysis of Fig. 3 reveals two relevant differences. (i) In the top panels, the Fermi level lies below the band maximum *and* below the crossing point of the split sp_z bands, i.e., in region II of Fig. 1. In contrast, it is always in region II of the p_xp_y states for the Ag alloys but above the band maximum for the sp_z states. (ii) Considering the Bi alloys, the splitting is strongly reduced in (b) $BiCu_2$ with respect to (d) $BiAg_2$.

The observed differences in the relative energy position of the Fermi level follow the charge transfer in the topmost layer. In Table I, we present results of our first-principles calculations for three of the investigated alloys. For the structure determination we use the Vienna *ab initio* simulation package. The semi-infinite surface system is simulated by a slab, where the atom positions can be relaxed both in-plane and in the perpendicular directions. First, the optimum in-plane lattice constant is calculated for an uncovered Ag slab. In a second step, for the system with the alloyed topmost layer, both the adatoms and the substrate atoms are allowed to relax in the so-determined two-dimensional unit cell. As to the band-structure calculation, in our self-consistent Korringa-Kohn-Rostoker (KKR) approach we used the Perdew-Wang exchange-correlation potential,[24] computed within muffin-tin spheres. Details are discussed elsewhere.[25]

The charge transfer Δn is determined from the charges Z_{mt} inside the muffin-tin spheres and is defined as $\Delta n = Z - Z_{mt}$, where Z is the atomic number. Therefore it is positive for a displacement of electronic charges from the alloy layer to the substrate layers and to the vacuum. The results computed around the noble-metal atoms show negligible variations with respect to the nominal atomic charge and are not reported in Table I. Whereas there is no general agreement among the published values of the relaxation for the three compounds, the trend of increasing relaxation from $SbAg_2$ to $BiAg_2$ to $BiCu_2$ is established in both experiment and theory, and in accordance with our findings. Sb/Ag(111) shows the smallest relaxation and consequently the charge transfer from the adatoms is comparatively low. As a result, the Fermi energy is located clearly above the band maximum for the sp_z states. For Bi/Ag(111), the relaxation is slightly larger than for Sb/Ag(111), which may be attributed to the larger atomic radius of Bi as compared to Sb. In this case, our calculation probably underestimates the actual relaxation, and this would explain the slightly too large binding energy of the sp_z bands found in our approach, since a larger outward relaxation would shift the sp_z states toward the Fermi level.[4] Due to the smaller lattice constant of Cu as compared to Ag, the relaxation for Bi/Cu(111) is considerably increased. The strong charge transfer shifts the sp_z states even further in energy and the Fermi level lies clearly in region II. In summary, we observe a correlation between the trends shown by relaxation, charge transfer, and the relative position of the Fermi level in the surface alloys.

A closeup of the interface bands around $\bar{\Gamma}$ is shown in Fig. 4 for [(a) and (c)] Sb/Cu(111) and [(b) and (d)] Bi/Cu(111) in the [(a) and (b)] $\bar{\Gamma}\bar{K}$ and [(c) and (d)] $\bar{\Gamma}\bar{M}$ directions. In the $SbCu_2$ maps three high-intensity features crossing the Fermi level can be identified and labeled with increasing numbers for increasing values of the Fermi vector k_F. The two at smaller k have negative effective masses and form hole pockets at $\bar{\Gamma}$. As anticipated, by analogy with Sb/Ag(111) it can be inferred that each one of these consists in fact of a pair of unresolved components ("1–2" and "3–4"). The additional feature ("5") near the image edges, at $k_x \simeq \pm 0.4$ Å^{-1} and $k_y \simeq \pm 0.35$ Å^{-1}, is a replica of the bulk Cu $4s$ band, backfolded by the $(\sqrt{3}\times\sqrt{3})R30°$ potential. For $BiCu_2$ four features can be observed [the umklapp signal 5 is too weak to be visible in (d)]. The splitting of the outer set (3–4, at $k_x \simeq \pm 0.28$ Å^{-1} and $k_y \simeq \pm 0.31$ Å^{-1}) is still too small to be detected but the inner set appears as two distinct bands, clearly distinguishable. The dashed parabolas superimposed to the images, crossing the Fermi level at $k_x = k_y = \pm 0.27$ Å^{-1}, indicate the edges of the surface-projected L gap in the bulk band structure, which shows up as a region of low intensity in the ARPES maps. The external (large k_F) branches of set 1–2 in $BiCu_2$ [Figs. 4(b) and 4(d)] are only visible inside the projected gap. Their intensity drops dramatically after crossing the gap boundaries, whereas the internal (small k_F) branches are still well visible outside the gap.

Even though for the Cu alloys region I of Fig. 1 cannot be accessed by photoemission, the large $1/\sqrt{E}$ slope of the DOS above the crossing point, discussed in the introduction, makes it possible to identify the band maximum by scanning tunneling spectroscopy (STS).[19] An STS investigation of the Bi/Cu(111) surface (shown in Fig. 5) locates the maximum at

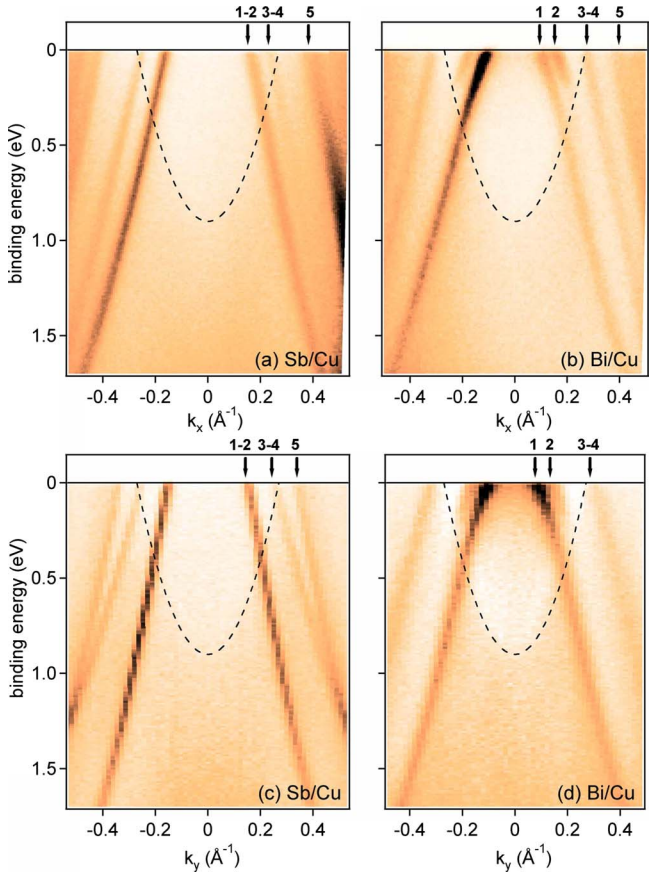

FIG. 4. (Color online) ARPES intensity maps for $SbCu_2$ and $BiCu_2$ along [(a) and (b)] $\bar{\Gamma}\bar{K}$ and [(c) and (d)] $\bar{\Gamma}\bar{M}$, measured at $T \simeq 40$ K. The dashed curves indicate the boundaries of the Cu L gap projected on the Cu(111) surface, extracted from Ref. 26.

~ 0.23 eV above the Fermi level. This can be used as input value for the fit of the data of Figs. 4(b) and 4(d). The best fit to the measured band dispersion is obtained for $m^\star \simeq -0.27 m_e$ and $k_0 \simeq 0.03$ Å^{-1}, which yields $E_R \simeq 15$ meV and $\alpha_R \simeq 1$ eV Å. We estimate for these values a quite large error bar of 20% because of the deviation from a parabolic dispersion and also because the two external branches of the band set are clearly visible only within a small (<200 meV) energy window, as discussed above.

The relevant quantities inferred from the data for the four alloys are summarized in Table II, limited to the sp_z bands.

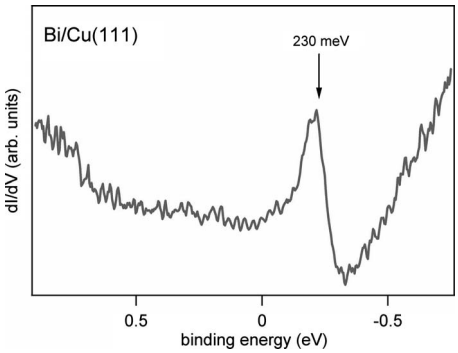

FIG. 5. STS spectrum of Bi/Cu(111), showing the density of states with a peak in correspondence of the maximum of the hybrid sp_z band.

Considering the wave-vector offset k_0, the measured SO splitting is about four times smaller for the Cu alloys, within the accuracy of our data and fitting. Although the presence of only two data points does not allow a definitive quantitative conclusion on the role played by the substrate atoms, we point out that the trend shown by the splitting size follows that of the SO parameter of the two substrates [ζ_{4p}(Cu) $=0.03$ eV vs ζ_{5p}(Ag)$=0.11$ eV].[27,28] It is actually reasonable that the strengths of the atomic SO interactions of both the substrate and the adsorbate are relevant for the final splitting since the wave functions are distributed over the entire surface-alloy layer, i.e., not exclusively located at Bi or Sb sites. Table III shows the calculated spectral weight of the sp_z states at the $\bar{\Gamma}$ crossing point, projected on the (Ag, Cu) sites, in the surface and the next subsurface layers. The relative weights N at the substrate atoms, normalized to the spectral weight at the (Bi, Sb) adatoms (=100%), are reported for the different layers s. In the bulk band gap, the spectral density computed within the KKR method can be safely associated with the sp_z bands. For all the considered systems the wave functions are strongly localized in the topmost layer, i.e., in the alloy layer while the subsurface sites carry altogether at most 22% of the spectral weight present at the adatom sites. This would point toward a negligible effect of the atomic SO coupling of the substrate atoms. However, the substrate atoms in the surface layer carry a considerable charge, e.g., more than 80% for Ag in $SbAg_2$ and this justifies the substrate-atom contribution to the band splitting.

A closer inspection of the Fermi surfaces shows the effect of the lattice potential on the band structure, which deviates

TABLE II. Characteristic quantities inferred from the surface-band dispersion of the four alloys, by columns: (1) effective mass $m^\star$, (2) wave-vector offset k_0, (3) Rashba energy E_R, (4) Rashba parameter α_R, (5) $\overline{\Gamma K}$ distance, and (6) Fermi vector k_F (two values are given for the two spin-split states). ◦ indicates values below the sensitivity of our measurements. For Sb/Cu, the value of $m^\star$ is missing since the band maximum is unknown in lack of STS data or calculations.

Alloy	$m^\star(m_e)$	k_0 (Å^{-1})	E_R (meV)	α_R (eV Å)	$\overline{\Gamma K}$ (Å^{-1})	k_F (Å^{-1})
Bi/Cu(111)	−0.27	0.03	15	1	0.95	0.10/0.16
Sb/Cu(111)		◦	◦	◦	0.95	0.15
Bi/Ag(111)	−0.35	0.13	200	3.05	0.84	*Undefined*
Sb/Ag(111)	−0.15	◦	◦	◦	0.84	*Undefined*

TABLE III. Calculated spectral weight of the sp_z states at the $\bar{\Gamma}$ crossing point, projected on the substrate atoms, in the surface layer s and in the first subsurface layers $s-1$, $s-2$, and $s-3$, relative to the spectral weight at the adsorbate atom sites.

Alloy	$N(s)$ (%)	$N(s-1)$ (%)	$N(s-2)$ (%)	$N(s-3)$ (%)
Sb/Ag(111)	82	20	2	<1
Bi/Ag(111)	66	12	1	<1
Bi/Cu(111)	52	9	2	<1

from the circular shape typical of a nearly free-electron band. In $SbCu_2$ [Fig. 6(a)] the Fermi surface consists of two hexagons both nearly degenerate and offset by 30° with respect to each other [bands 1–2 and 3–4 in Figs. 4(a) and 4(c)]. The inner hexagon, corresponding to the 1–2 bands, has the same orientation as the BZ, in agreement with what found for $SbAg_2$.[5] Around the two hexagons, the backfolded Cu 4s band forms a David-star shape, similar to the case of a Xe monolayer on Cu(111).[29] In $BiCu_2$ [Fig. 6(b)] once again the outer hexagon [bands 3–4 in Figs. 4(a) and 4(c)] cannot be resolved in its two components, whereas the inner, nearly circular Fermi-surface sheet, appears clearly split [bands "1" and "2" in Figs. 4(b) and 4(d)], as expected from the simple picture of Fig. 1.

IV. CONCLUSIONS

We have presented an ARPES investigation of the Bi/Cu(111) and Sb/Cu(111) surface alloys and have carried out a comparison with the recent results obtained on the equivalent alloys on Ag(111). The distinctive features of the band structure are common to all four systems. The size of the spin splitting is smaller in the Cu alloys than in the Ag alloys and vanishingly small for Sb/Cu(111). The relative decrease observed between Bi/Ag(111) and Bi/Cu(111) is in fair agreement with the reduction in the atomic spin-orbit parameter between the two substrates. At variance with the Ag(111) counterparts, the Fermi level is located in the region below the crossing point of the split bands.

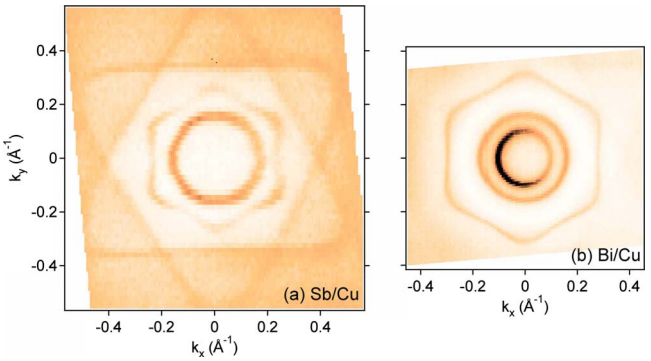

FIG. 6. (Color online) Measured Fermi surfaces of (a) Sb/Cu(111) and (b) Bi/Cu(111). The horizontal axis is along the $\bar{\Gamma}\bar{K}$ direction of the alloys.

ACKNOWLEDGMENTS

This work was supported by the Swiss National Science Foundation, by the MaNEP NCCR, and by the Bundesministerium für Bildung und Forschung (BMBF) under Grant No. 05KS7WW1. Preliminary measurements have been performed at the Synchrotron Radiation Center in Madison, funded by the National Science Foundation under Award No. DMR-0537588. A.B. thanks the Alexander von Humboldt foundation for financial support.

[1] D. Pacilé, C. R. Ast, M. Papagno, C. Da Silva, L. Moreschini, M. Falub, A. P. Seitsonen, and M. Grioni, Phys. Rev. B **73**, 245429 (2006).
[2] C. R. Ast, J. Henk, A. Ernst, L. Moreschini, M. C. Falub, D. Pacilé, P. Bruno, K. Kern, and M. Grioni, Phys. Rev. Lett. **98**, 186807 (2007).
[3] J. Premper, M. Trautmann, J. Henk, and P. Bruno, Phys. Rev. B **76**, 073310 (2007).
[4] G. Bihlmayer, S. Blügel, and E. V. Chulkov, Phys. Rev. B **75**, 195414 (2007).
[5] L. Moreschini *et al.*, Phys. Rev. B **79**, 075424 (2009).
[6] L. Petersen and P. Hedegåard, Surf. Sci. **459**, 49 (2000).
[7] G. Bihlmayer, Y. M. Koroteev, P. M. Echenique, E. V. Chulkov, and S. Blügel, Surf. Sci. **600**, 3888 (2006).
[8] S. LaShell, B. A. McDougall, and E. Jensen, Phys. Rev. Lett. **77**, 3419 (1996).
[9] H. Cercellier, C. Didiot, Y. Fagot-Revurat, B. Kierren, L. Moreau, D. Malterre, and F. Reinert, Phys. Rev. B **73**, 195413 (2006).
[10] G. H. Nicolay, F. Reinert, S. Hüfner, and P. Blaha, Phys. Rev. B **65**, 033407 (2001).
[11] E. A. Soares, C. Bittencourt, V. B. Nascimento, V. E. de Carvalho, C. M. C. de Castilho, C. F. McConville, A. V. de Carvalho, and D. P. Woodruff, Phys. Rev. B **61**, 13983 (2000).
[12] D. Kaminski, P. Poodt, E. Aret, N. Radenovic, and E. Vlieg, Surf. Sci. **575**, 233 (2005).
[13] H. Xiao, X. Zu, X. He, and F. Gao, Chem. Phys. **325**, 519 (2006).
[14] D. Woodruff and J. Robinson, J. Phys.: Condens. Matter **12**, 7699 (2000).
[15] K. Umezawa, H. Takaoka, S. Hirayama, S. Nakanishi, and W. M. Gibson, Curr. Appl. Phys. **3**, 71 (2003).
[16] C. Nagl, O. Haller, E. Platzgummer, M. Schmid, and P. Varga, Surf. Sci. **321**, 237 (1994).
[17] Y. A. Bychkov and E. I. Rashba, JETP Lett. **39**, 78 (1984).
[18] E. Cappelluti, C. Grimaldi, and F. Marsiglio, Phys. Rev. Lett. **98**, 167002 (2007).
[19] C. R. Ast, G. Wittich, P. Wahl, R. Vogelgesang, D. Pacilé, M. C. Falub, L. Moreschini, M. Papagno, M. Grioni, and K. Kern, Phys. Rev. B **75**, 201401(R) (2007).

[20] D. S. Saraga and D. Loss, Phys. Rev. B **72**, 195319 (2005).
[21] C. R. Ast, D. Pacilé, M. Papagno, T. Gloor, F. Mila, S. Fedrigo, G. Wittich, K. Kern, H. Brune, and M. Grioni, Phys. Rev. B **73**, 245428 (2006).
[22] S. A. de Vries, W. J. Huisman, P. Goedtkindt, M. J. Zwanenburg, S. L. Bennett, I. K. Robinson, and E. Vlieg, Surf. Sci. **414**, 159 (1998).
[23] T. Hirahara, T. Komorida, A. Sato, G. Bihlmayer, E. V. Chulkov, K. He, I. Matsuda, and S. Hasegawa, Phys. Rev. B **78**, 035408 (2008).
[24] J. P. Perdew and Y. Wang, Phys. Rev. B **45**, 13244 (1992).
[25] H. Mirhosseini, J. Henk, A. Ernst, S. Ostanin, C.-T. Chiang, P. Yu, A. Winkelmann, and J. Kirschner, Phys. Rev. B **79**, 245428 (2009).
[26] F. Reinert, G. Nicolay, S. Schmidt, D. Ehm, and S. Hüfner, Phys. Rev. B **63**, 115415 (2001).
[27] C. E. Moore, *Atomic Energy Levels*, NSRDS-NBS No. 35, Vol. III (Natl. Bur. Stand., Washington, DC, 1970).
[28] Y. Yafet, in *Solid State Physics* edited by F. Seitz and D. Turnbull, (Academic Press, New York 1963), Vol. 14, p. 1.
[29] F. Forster, S. Hüfner, and F. Reinert, J. Phys. Chem. B **108**, 14692 (2004).